Available online at www.sciencedirect.com
SCIENCE DIRECT®
Journal of Nuclear Materials 346 (2005) 208–219
journal of nuclear materials
www.elsevier.com/locate/jnucmat

A new model of grain growth kinetics in UO_2 fuel pellets. Part 1: Grain growth kinetics controlled by grain face bubble migration

M.S. Veshchunov *

Russian Academy of Sciences, Nuclear Safety Institute (IBRAE), 52, B. Tulskaya, Moscow 115191, Russia

Received 1 February 2005; accepted 10 June 2005

Abstract

A new mechanism of the lenticular grain face bubble migration which controls the bubble mobility and determines the drag force exerted on the grain boundary, is developed. It is shown that besides a more complicated (so called 'lenticular') shape of grain face bubbles, the migration mechanism of these bubbles might be essentially different from the intragranular bubbles, owing to their specific location on and interaction with a grain boundary. The model is validated against tests on grain growth kinetics during steady irradiation exposure and during post-irradiation annealing of UO_2 fuel samples, and allows explanation of a strong retarding effect of irradiation on the grain growth observed in these tests.

1. Introduction

Grain growth is the process by which the mean grain size of aggregates of crystals increases. The driving force for this process results from the decrease in free energy which accompanies reduction in total grain boundary area. Second-phase inclusions act as pinning agents to grain boundaries since the attachment of an inclusion reduces the total boundary energy by an amount equal to the specific surface energy times the area occupied by the inclusions. If the inclusions are relatively immobile, a boundary pinned at an inclusion (with the pinning force F_m) can only move by breaking free. This occurs when the driving force ΔG for the boundary migration exceeds the pinning force $n_b F_m$ exerted by n_b bubbles (per unit boundary square) on the boundary. In the case of mobile second-phase inclusions (e.g. gas bubbles or pores), they migrate along with the boundaries, in some circumstances giving a boundary migration rate controlled by the movement of the second-phase particles.

Speight and Greenwood [1] proposed a grain growth theory that includes the sweeping of entrapped microbubbles by the front of an advancing grain boundary. The basic postulate of their theory is that small bubbles, because they exert a minimal drag force on an advancing grain surface, are swept along with the moving boundary, whereas large bubbles, because of their higher drag, can detach from the advancing surface.

* Tel.: +7 095 955 2218; fax: +7 095 958 0040.
E-mail address: vms@ibrae.ac.ru

0022-3115/$ - see front matter © 2005 Elsevier B.V. All rights reserved.
doi:10.1016/j.jnucmat.2005.06.011

This theory was applied in the VICTORIA code [2] to modelling grain growth and grain boundary sweeping. Various types of grain boundary pores and bubbles (i.e. grain face, edge and corner) which exert different drag forces owing their different shapes and sizes were additionally considered in the code following Rest [3]. In this approach the drag force exerted by an attached bubble moving along with the boundary is calculated as the pinning force F_m, evaluated for immobile inclusions. For this reason, the grain boundary velocity is determined in [2] by the resulting force $\Delta G - n_b F_m$ acting on the boundary and the grain boundary mobility.

Naturally, such an approach is valid only for estimation of the pinning effect on the boundary exerted by immobile inclusions. In the general case the resulting drag force can be significantly lower and essentially dependent on the inclusions' mobility. For this reason, the drag force should be calculated self-consistently with the grain boundary velocity as proposed by Nichols [4] (see Section 2).

However, Nichols analysed a simplified problem of a single boundary movement representing an average behaviour of an aggregate of crystals, without consideration of a real size distribution of grains and their coalescence.

Such a consideration can be done in the framework of Hillert's mean-field approach [5] and is performed in the present paper (Section 2). Besides, an additional consideration proposed by Rest [3] of various types of grain boundary pores and bubbles (i.e. grain face, edge and corner) which exert different drag forces owing to their different shapes and sizes, is carried out.

Another deficiency of Nichols' analysis [4] is associated with consideration of a retarding effect using the standard mechanisms of bubble mobility derived by Shewmon [6] for intragranular bubbles. However, besides a more complicated (so called 'lenticular') shape of grain face bubbles, the migration mechanism of these bubbles might be essentially different from that of the intragranular bubbles, owing to their specific location on and interaction with a grain boundary. A new mechanism of the lenticular grain face bubble migration which controls the bubble mobility and determines the drag force exerted on the grain boundary, will be presented in Section 3.

After implementation of the new model in the mechanistic code MFPR which is designed for modelling fission product release from irradiated UO_2 fuel and developed in close co-operation between IBRAE (Moscow) and IRSN (Cadarache, France) [7–9], simulation of the kinetics of UO_2 grain growth under steady irradiation conditions (measured in Turnbull's tests [10]) and during post-irradiation annealing of UO_2 samples with different irradiation exposures (measured in MacEwan and Hayayshi's tests [11]), are performed in Section 4.

2. Bubbles retarding effect in mean field approximation for grain size distribution

Burke and Turnbull [12] deduced a parabolic relationship for grain growth kinetics. They modelled migration of a boundary as occurring by atom transport across the boundary due to a surface curvature and pressure gradient between grains. In this approach the driving force applied to the boundary of a spherical grain with radius R_{gb} is written as

$$\Delta G = \frac{\xi \gamma_{gb}}{R_{gr}}, \tag{1}$$

where γ_{gb} is the surface energy of the boundary, and $\xi \approx 1$–2 is a geometric factor.

Under simplifying assumption $R_{gr} = \bar{R}_{gr}$, where $\bar{R}_{gr}$ is the mean grain radius, the mean grain boundary velocity is given by equation [12]:

$$v_{gb}^{(0)} = \frac{d\bar{R}_{gr}}{dt} = u\Delta G = \frac{M'}{\bar{R}_{gr}}, \tag{2}$$

where u is the grain boundary mobility, and $M' = u\gamma_{gb}\xi$. After integration, Eq. (2) results in the parabolic grain growth.

A more appropriate treatment of the grain growth problem with consideration of grain coalescence was performed by Greenwood [13], who modified Eq. (1) to the form:

$$\Delta G = \xi \gamma_{gb}\left(\frac{1}{R_c} - \frac{1}{R_{gb}}\right), \tag{3}$$

where R_c is the critical radius which varies with time. Therefore the grain boundary velocity of a spherical grain with the radius R_{gb} is given by equation [13]:

$$v_{gb}^{(0)} = \frac{dR_{gr}}{dt} = u\Delta G = M'\left(\frac{1}{R_c} - \frac{1}{R_{gr}}\right). \tag{4}$$

Grains grow or collapse depending on whether $R_{gr} > R_c$ or $R_{gr} < R_c$, respectively.

Using Eq. (4), the kinetics become identical with those for Ostwald ripening of a distribution of second phase particles, with interphase reactions controlling the rate at which large particles grow at the expense of smaller ones. Hillert [5] used previous analysis of Lifshitz and Slyozov [14] for Ostwald ripening to obtain parabolic kinetics for grain growth.

According to Hillert's theory [5] the critical radius satisfies equation:

$$\frac{dR_c}{dt} = \frac{M'}{8}\frac{1}{R_c}, \tag{5}$$

whereas the mean grain radius $\bar{R}_{gr}$ is related to the critical radius R_c by

$$\bar{R}_{gr} = (8/9)R_c. \tag{6}$$

So, for the mean grain growth velocity this results in:

$$\bar{v}_{\rm gb}^{(0)} = \frac{{\rm d}\overline{R}_{\rm gr}}{{\rm d}t} = M\frac{1}{\overline{R}_{\rm gr}}, \tag{7}$$

where

$$M = \frac{8M'}{81} = \frac{8}{81}u\gamma_{\rm gb}\xi. \tag{8}$$

Hence, in comparison with the simplified approach [12], the effective mobility of the mean grain boundary migration in Eq. (7) turns out to be one order of magnitude smaller than in Eq. (2).

However, Eqs. (2) and (7) were derived without intergranular bubbles taken into consideration. On the other hand, Nichols [4] considered the retarding effect of bubbles on a separately moving grain boundary and showed that in presence of the attached bubbles the grain boundary motion is governed by the net force $\Delta G - Fn_{\rm b}$, where F is the force applied to a separate bubble and $n_{\rm b}$ is the surface concentration of bubbles, moving along with the grain boundary. Therefore the grain boundary velocity was calculated modifying Eq. (2) as

$$v_{\rm gb} = u(\Delta G - Fn_{\rm b}) = \frac{v_{\rm gb}^{(0)}}{\Delta G}(\Delta G - Fn_{\rm b}). \tag{9}$$

Simultaneously, the bubble velocity $v_{\rm b}$ is equal to $v_{\rm gb}$, until the bubble is attached to the boundary [1]:

$$v_{\rm b} = bF = v_{\rm gb}, \tag{10}$$

where

$$b = \frac{2D_{\rm b}}{kT}, \tag{11}$$

and $D_{\rm b}$ is the bubble diffusion coefficient (dependent on the bubble radius $R_{\rm b}$).

Using Eqs. (9)–(11) the force F can be calculated as

$$F = \frac{v_{\rm gb}^{(0)}\Delta G/n_{\rm b}}{v_{\rm gb}^{(0)} + b\Delta G/n_{\rm b}}, \tag{12}$$

Therefore, one derives the equation for the grain boundary velocity [4]:

$$v_{\rm gb} = \frac{v_{\rm gb}^{(0)}b\Delta G/n_{\rm b}}{v_{\rm gb}^{(0)} + b\Delta G/n_{\rm b}} = \frac{ub/n_{\rm b}}{u + b/n_{\rm b}}\Delta G. \tag{13}$$

Nichols' approach can be generalised to a more realistic description of grain growth with consideration of size distribution and coalescence of grains. In Hillert's approach using the same procedure as for derivation of Eq. (7) from Eq. (4), one can obtain for the mean grain velocity a new relationship instead of Eq. (13):

$$\bar{v}_{\rm gb} = \frac{8}{81}\frac{\xi\gamma_{\rm gb}}{\overline{R}_{\rm gr}}\left(\frac{u(b/n_{\rm b})}{u + (b/n_{\rm b})}\right), \tag{14}$$

or, after substitution of Eq. (8):

$$\bar{v}_{\rm gb} = \bar{v}_{\rm gb}^{(0)}\left(\frac{(b/n_{\rm b})}{\left(\bar{v}_{\rm gb}^{(0)}\overline{R}_{\rm gr}\right)\frac{81}{8\xi\gamma_{\rm gb}} + (b/n_{\rm b})}\right). \tag{15}$$

It is important to note from Eq. (15) that pore (bubble) parameters control the boundary movement when $(\bar{v}_{\rm gb}^{(0)}\overline{R}_{\rm gr})\frac{81}{8\xi\gamma_{\rm gb}} \gg (b/n_{\rm b})$. Comparing Eq. (15) with Eq. (13) one can see that in the advanced model (with application of the Hillert's approach to consideration of grain size distribution) this occurs significantly earlier when $\overline{R}_{\rm gr} \gg 0.1\frac{(b/n_{\rm b})\xi\gamma_{\rm gb}}{\bar{v}_{\rm gb}^{(0)}}$, i.e. at a grain size one order of magnitude smaller than in the simplified approach [4].

To take into account different kinds of bubbles on the grain boundary, i.e. face (f), edge (e) and corner (c) bubbles, relationship similar to Eq. (10) should be applied to each kind of bubbles [3]:

$$v_{\rm gb} = v_{\rm f} = b_{\rm f}F_{\rm f} = v_{\rm e} = b_{\rm e}F_{\rm e} = v_{\rm c} = b_{\rm c}F_{\rm c}, \tag{16}$$

therefore,

$$F_{\rm e} = \frac{b_{\rm f}}{b_{\rm e}}F_{\rm f}, \quad F_{\rm c} = \frac{b_{\rm f}}{b_{\rm c}}F_{\rm f}. \tag{17}$$

The net force acting on the boundary takes the form:

$$\Delta G - n_{\rm f}F_{\rm f} - n_{\rm e}F_{\rm e} - n_{\rm c}F_{\rm c} = \Delta G - F_{\rm f}\left(n_{\rm f} + n_{\rm e}\frac{b_{\rm f}}{b_{\rm e}} + n_{\rm c}\frac{b_{\rm f}}{b_{\rm c}}\right), \tag{18}$$

this results in the following relationship generalising equation (13):

$$v_{\rm gb} = \frac{v_{\rm gb}^{(0)}}{1 + \frac{v_{\rm gb}^{(0)}}{\Delta G}(n_{\rm f}b_{\rm f}^{-1} + n_{\rm e}b_{\rm e}^{-1} + n_{\rm c}b_{\rm c}^{-1})}. \tag{19}$$

Finally, for the mean grain boundary velocity one obtains in a similar way to derivation of Eq. (15):

$$\bar{v}_{\rm gb} = \frac{v_{\rm gb}^{(0)}}{1 + \frac{81v_{\rm gb}^{(0)}\overline{R}_{\rm gr}}{8\xi\gamma_{\rm gb}}\left(n_{\rm f}b_{\rm f}^{-1} + n_{\rm e}b_{\rm e}^{-1} + n_{\rm c}b_{\rm c}^{-1}\right)}. \tag{20}$$

3. New mechanism for grain face bubble migration and drag force exerted on a moving boundary

In accordance with [4,6], the mobility of a spherical intragranular bubble is determined by various migration mechanisms:

$$b \propto R_{\rm b}^{-n}, \tag{21}$$

where $n = 3$ for the mechanisms of lattice diffusion and gas phase transport, and $n = 4$ for the surface diffusion mechanism.

Presumably the same migration mechanisms can be also applied to the grain face bubbles with some

renormalisation of the proportionality coefficient in Eq. (21), owing to a more complicated lenticular form of these bubbles (see below Section 3.3). However, a more profound difference from free intragranular bubbles arises on grain faces, which can significantly reduce the intergranular bubble mobility and thus migration velocity of the grain boundary. This new rate determining mechanism of bubble migration will be presented in this Section.

3.1. Phenomenological consideration

Before presenting a more detailed 'microscopic' consideration of the grain boundary migration with attached bubbles, a phenomenological approach to calculation of the retarding force exerted by bubbles on the moving boundary will be presented.

As above mentioned, the driving force for the boundary migration can be derived from the pressure gradient across the boundary arising from its curvature given by Eq. (1). This pressure gradient between the two adjacent grains provides different boundary conditions also for gas bubbles in these grains; in particular, an additional external hydrostatic pressure $p_{\rm ext} = \Delta G$ is applied to the spherical segment of the lenticular bubble surface in the shrinking grain.

In order to clarify the nature of the drag force exerted on the grain boundary by an attached bubble, at first a simplified limiting case of a complete equilibrium of the lenticular bubble with both grains (shrinking and growing) separated by the boundary under steady-state conditions, will be considered.

In this limiting case

$$\Delta p_2 \equiv p_{\rm b} - \frac{2\gamma_{\rm s}}{R_2} = 0, \tag{22}$$

$$\Delta p_1 \equiv p_{\rm b} - \frac{2\gamma_{\rm s}}{R_1} - \Delta G = 0, \tag{23}$$

where $p_{\rm b}$ is the internal bubble pressure, R_1 and R_2 are the curvature radii of the two surface segments of the bubble.

One can see from Eqs. (22) and (23) that the curvature radii of the two bubble surfaces are different, this induces different contact angles θ_1 and θ_2 with the grain boundary:

$$R_1 \cdot \sin\theta_1 = R_2 \cdot \sin\theta_2 = \rho_{\rm b}, \tag{24}$$

where $\rho_{\rm b}$ is the projected radius of the bubble in the plain of the boundary.

Assuming a balance between the surface tension forces in the plane of the grain boundary under steady-state conditions:

$$\gamma_{\rm gb} = \gamma_{\rm s}(\cos\theta_1 + \cos\theta_2), \tag{25}$$

one can calculate a net force exerting by the bubble on the grain boundary in the normal to the grain boundary direction (see Fig. 1):

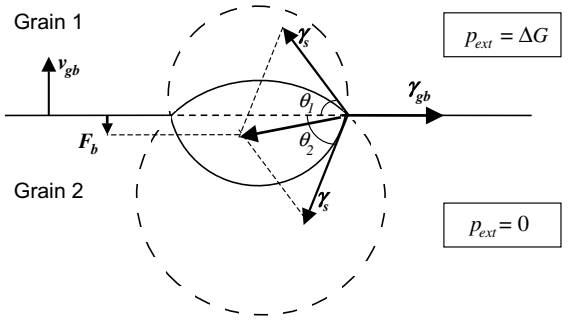

Fig. 1. Determination of the drag force exerted by attached lenticular bubble on moving grain boundary.

$$2\pi\rho\gamma_{\rm s}(\sin\theta_2 - \sin\theta_1) = F_{\rm b}. \tag{26}$$

Substituting Eqs. (22)–(25) in Eq. (26), one gets:

$$F_{\rm b} = \Delta G \cdot \pi\rho_{\rm b}^2, \tag{27}$$

and therefore, in accordance with Eq. (9), the driving force for the grain boundary migration is reduced proportionally to the reduction of the grain boundary area owing to its coverage with bubbles:

$$\Delta G' = \Delta G - F_{\rm b} n_{\rm b} = \Delta G(1 - n_{\rm b} \cdot \pi\rho_{\rm b}^2). \tag{28}$$

The above presented consideration of the bubble equilibrium with the two grains can be justified only in the case when the rate determining process of bubble mobility is infinitely fast in comparison with the grain boundary migration. In a more general case of a finite bubble mobility, a complete equilibrium between the bubble and the two grains is not attained, hence Eqs. (22) and (23) are not anymore valid. It is straightforward to show that in order to uphold a coherent migration of the grain boundary and the attached bubble in this case, the values Δp_1 and Δp_2 become non-zero and obey the relationship:

$$\Delta p_1 = p_{\rm b} - \frac{2\gamma_{\rm s}}{R_1} - \Delta G = -\Delta p_2 = \frac{2\gamma_{\rm s}}{R_2} - p_{\rm b} = \varepsilon > 0. \tag{29}$$

Indeed, during a time interval $\mathrm{d}t$ the grain boundary moves over a distance $v_{\rm gb}\,\mathrm{d}t$. If the bubble is 'frozen' at its position, the volume of the upper part of the bubble (see Fig. 2) will be decreased by a value $\mathrm{d}V = \pi\rho_{\rm b}^2 v_{\rm gb}\,\mathrm{d}t$, whereas the volume of the lower part will be increased by the same value $\mathrm{d}V$. In order to sustain the bubble migration with the grain boundary velocity $v_{\rm gb}$, vacancy fluxes along the upper and lower surfaces of the grain boundary, $J_{\rm v}^{(1)}$ and $J_{\rm v}^{(2)}$, should compensate these volume variations:

$$J_{\rm v}^{(1)} 2\pi\rho_{\rm b}\Omega\,\mathrm{d}t = -J_{\rm v}^{(2)} 2\pi\rho_{\rm b}\Omega\,\mathrm{d}t = \mathrm{d}V = \pi\rho_{\rm b}^2 v_{\rm gb}\,\mathrm{d}t, \tag{30}$$

where Ω is the vacancy volume. It is assumed that each of the vacancy fluxes ($J_{\rm v}^{(1)}$ or $J_{\rm v}^{(2)}$) occurs in a thin surface layer with a thickness $w \approx 0.5$ nm of the corresponding

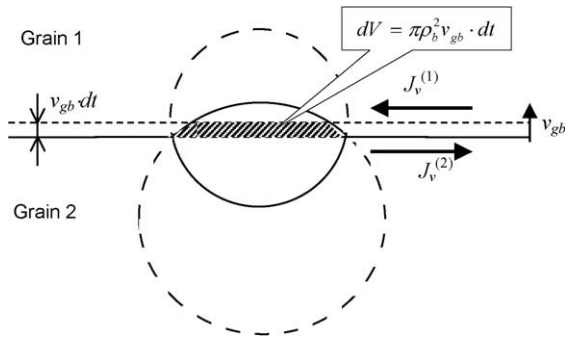

Fig. 2. Determination of vacancy fluxes along the grain boundary in two adjacent grains providing relocation of a lenticular bubble coherently with the grain boundary.

grain (grain 1 or grain 2), characterised by a relatively high self-diffusion coefficient D_{gb}.

These fluxes will be calculated in the following Section 3.2, nevertheless, from the physical point of view (confirmed by calculations presented below) it is clear that the values of $J_v^{(1)}$ and $J_v^{(2)}$ are determined by the pressure differences Δp_1 and Δp_2, respectively, which should obey condition $\Delta p_1 = -\Delta p_2$, Eq. (29), in order to sustain relationship $J_v^{(1)} = -J_v^{(2)}$, Eq. (30).

Eqs. (24)–(26) are still valid for the considered case of a non-equilibrium bubble with the steady-state lenticular shape, and along with Eq. (29) determine the retarding force:

$$F_b = 2\pi\rho\gamma_s(\sin\theta_2 - \sin\theta_1) = \pi\rho_b^2(\Delta G + 2\varepsilon). \tag{31}$$

Substitution Eq. (31) in Eq. (9) results in:

$$v_{gb} = u_{gb}\left[\Delta G(1 - n_b \cdot \pi\rho_b^2) - 2\varepsilon n_b \cdot \pi\rho_b^2\right]. \tag{32}$$

Superposition of Eqs. (32) and (30) with explicitly calculated fluxes $J_v^{(1)}$ and $J_v^{(2)}$ as a function of ε will finally determine the migration of the grain boundary with attached bubbles.

The same result, Eq. (32), derived in the present subsection in phenomenological approach (i.e. by consideration of mechanical forces, acting on the boundary and bubbles), can be obtained in a more accurate microscopic approach based on self-consistent calculation of vacancy fluxes across and along the grain boundary, which will be presented in the following Section 3.2.

3.2. Microscopic consideration

In accordance with Cole et al. [15], migration of a grain boundary of a growing grain takes place in steps of one interatomic spacing a as atoms transfer from the neighbouring grain across the boundary under the pressure difference ΔG across the boundary:

$$v_{gb}^{(0)} = \frac{2\upsilon a\Omega}{kT}\Delta G \exp\left(-\frac{Q}{kT}\right) \equiv u_{gb}\Delta G, \tag{33}$$

where υ is the atomic oscillation frequency on the grain boundary, Q is the activation energy for self-diffusion in the grain boundary, Ω is the atomic volume. The grain boundary mobility $u_{gb} = \frac{2\upsilon a\Omega}{kT}\exp(-\frac{Q}{kT})$, can be also evaluated following Burke and Turnbull [12] as

$$u_{gb} = \frac{D_{gb}\Omega}{2wkT}, \tag{34}$$

where $2w \approx 1$ nm is the thickness of the grain boundary, D_{gb} is the self-diffusion coefficient in the grain boundary.

The above described process of atomic jumps can be equivalently considered as translations of vacancies from the growing grain to the adjacent one with the same rate as translations of atoms in the opposite direction. The corresponding flux of vacancies $\tilde{J}_v^{(0)}$ in the normal to the grain boundary direction is uniform over the grain boundary surface (with the total area S) and thus determines the grain boundary relocation during the time interval dt, in accordance with the following relationship: $\tilde{J}_v^{(0)}\Omega S\,dt = S\,dx$. Therefore, the grain boundary migration velocity $v_{gb}^{(0)} = dx/dt$ can be represented in the form $v_{gb}^{(0)} = \tilde{J}_v^{(0)}\Omega$, and thus:

$$\tilde{J}_v^{(0)} = u_{gb}\Delta G/\Omega. \tag{35}$$

In the presence of attached bubbles with the surface coverage n_b and mean projected radius ρ_b, the vacancy flux takes place across the reduced surface of the grain boundary $S(1 - n_b\pi\rho_b^2)$. In the limiting case (corresponding to an infinite bubble mobility, or $\varepsilon \to 0$), when the lenticular bubble attains equilibrium with both grains separated by the boundary (see Eqs. (22) and (23)), the vacancy flux is still uniform over the reduced grain boundary surface, and thus, Eq. (35) can be used in the balance equation:

$$v_{gb}^{(0)}S = \tilde{J}_v^{(0)}\Omega S(1 - n_b\pi\rho_b^2). \tag{36}$$

Therefore, in this case the grain boundary velocity is calculated as

$$v_{gb}^{(0)} = u_{gb}\Delta G(1 - n_b \cdot \pi\rho_b^2), \tag{37}$$

in agreement with Eq. (28).

In a more general case of a limited bubble mobility when a complete equilibrium between the bubble and the grains is not attained and $\varepsilon > 0$, a spatial variation of the vacancy chemical potential over the grain boundary faces takes place. On the one hand, this chemical potential variation induces the vacancy fluxes to (from) the bubble along the upper (lower) surface of the grain boundary, $J_v^{(1)}$ and $J_v^{(2)}$, introduced in Eq. (30). On the other hand, the pressure drop across the boundary becomes also non-uniform over the grain face area; this modifies Eq. (37). In order to calculate the total vacancy flux across the boundary in this case, one should self-consistently consider the vacancy transport along and across the grain boundary, on the base of calculation

of the spatial variation of the vacancy chemical potential.

As shown by Speight and Beere [16], variation of the surface chemical potential $\mu(r) = \sigma_{nn}(r)\Omega$ in a grain reflects exactly the steady state distribution of normal stresses over the grain boundary area unoccupied by bubbles. In the currently considered problem with a moving grain boundary under pressure difference across the boundary, such a conclusion should be generalised and independently applied to each of the two adjacent grains, $\mu_{1,2}(r) = \sigma^{(1,2)}_{nn}(r)\Omega$. The integral of these stresses over the area (with the mean radius $R_c \approx (\pi n_b)^{-1/2}$) associated with one bubble must equal the total load applied to each face of the grain boundary. Hence, following [16], one obtains:

$$\Omega^{-1}\int_{\rho_b}^{R_c}\mu_{1,2}(r)2\pi r\,dr = \sigma_{1,2}\pi R_c^2 - \left(\frac{2\gamma_s}{R_{1,2}} - p_b\right)\pi\rho_b^2, \tag{38}$$

where the first term on the r.h.s. arises from the normal stresses $\sigma_{1,2}$ at each of two surfaces of the grain boundary in the absence of attached bubbles. In the presently considered case these stresses uphold the pressure gradient ΔG across the grain boundary, i.e.

$$\sigma_2 = \sigma_1 + \Delta G. \tag{39}$$

The second term on the r.h.s. of Eq. (38) expresses the force which the bubble surface tension exerts on the boundary. This term can be calculated as the integral of the normal stress on the lenticular bubble surface $\mu_{1,2}(R_{1,2},\theta) = \sigma^{(1,2)}_{nn}(\theta)\Omega = \left(\frac{2\gamma_s}{R_{1,2}} - p_b\right)\Omega$ over the corresponding surface segment of the bubble: $\int \sigma^{(1,2)}_{nn}(R_{1,2})\,dS_{1,2} = \left(\frac{2\gamma_s}{R_{1,2}} - p_b\right)\pi\rho_b^2$.

As illustrated in Fig. 3, the chemical potential gradients along the grain face surfaces, $\nabla_S\mu_1$ and $\nabla_S\mu_2$, determine the vacancy surface fluxes $J_v^{(1)}$ and $J_v^{(2)}$, introduced in Eq. (30), whereas the chemical potential drop across the grain boundary $\delta\mu(r) = \mu_2(r) - \mu_1(r)$ determines the vacancy flux across the grain boundary:

$$\widetilde{J}_v(r) = u_{gb}\delta\mu(r)/\Omega^2. \tag{40}$$

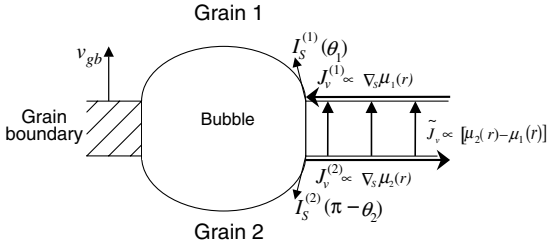

Fig. 3. Schematic representation of vacancy fluxes along and across the grain boundary.

Integrating this flux over the grain boundary area unoccupied by bubbles and using Eq. (38) one can calculate the grain boundary velocity:

$$\begin{aligned} v_{gb} &= \frac{u_{gb}}{\Omega\pi R_c^2}\int_{\rho_b}^{R_c}(\mu_2(r) - \mu_1(r))2\pi r\,dr \\ &= u_{gb}n_b\left[(\sigma_2 - \sigma_1)\pi R_c^2 - \left(\frac{2\gamma_s}{R_2} - \frac{2\gamma_s}{R_1}\right)\pi\rho_b^2\right]. \end{aligned} \tag{41}$$

The second term on the r.h.s. of Eq. (41) is calculated from Eq. (29):

$$\frac{2\gamma_s}{R_2} - \frac{2\gamma_s}{R_1} = 2\varepsilon + \Delta G. \tag{42}$$

Substitution of Eqs. (39) and (42) in Eq. (41) results in:

$$v_{gb} = u_{gb}\left|\Delta G(1 - n_b\cdot\pi\rho_b^2) - 2\varepsilon n_b\cdot\pi\rho_b^2\right|, \tag{43}$$

which exactly coincides with Eq. (32).

An additional relationship between v_{gb} and ε can be obtained from the balance equation, Eq. (30), if the surface vacancy fluxes $J_v^{(1)}$ and $J_v^{(2)}$ are properly ascertained. These fluxes obey the continuity equations on each face of the grain boundary, which in the system of coordinates moving along with the grain boundary take the form:

$$\vec{\nabla}_s\cdot\vec{J}_v^{(1,2)} \pm \widetilde{J}_v(r) \mp v_{gb}\Omega^{-1} = 0,$$

or

$$\frac{D_{gb}w\Omega}{kT}\nabla_s^2\mu_{1,2} \pm \frac{u_{gb}(\mu_2 - \mu_1)}{\Omega} \mp v_{gb} = 0, \tag{44}$$

with the boundary conditions:

$$\left(\frac{d\mu_{1,2}}{dr}\right)_{r=R_c} = 0 \quad\text{and}\quad \mu_{1,2}(\rho_b) = \left(\frac{2\gamma_s}{R_{1,2}} - p_b\right)\Omega. \tag{45}$$

It is straightforward to see that integration of Eq. (44) over the surface non-occupied with the bubbles, directly results in the first part of Eq. (41), if Eq. (30) is valid.

Solution of Eqs. (44) and (45) is presented in Appendix A and determines the vacancy fluxes at the bubble surface:

$$\begin{aligned} J_v^{(1)} = -J_v^{(2)} &= \frac{D_{gb}w\Omega}{2kT}\left(\Delta G + 2\varepsilon - \frac{v_{gb}}{u_{gb}}\right) \\ &\times \chi\frac{K_1(\chi\rho_b)I_1(\chi R_c) - I_1(\chi\rho_b)K_1(\chi R_c)}{I_0(\chi\rho_b)K_1(\chi R_c) + K_0(\chi\rho_b)I_1(\chi R_c)}, \end{aligned} \tag{46}$$

where $\chi = \sqrt{2u_{gb}kT/D_{gb}w\Omega}$, and $I_{0,1}(x)$ and $K_{0,1}(x)$ represent the first and the second modified Bessel functions of the zeroth and first kind, respectively.

Substitution of Eq. (46) in Eq. (30) results in the additional relationship for the grain boundary velocity:

$$\begin{aligned} v_{gb} = (\Delta G + 2\varepsilon)\pi\rho_b^2\Bigg[&\frac{D_{gb}w\Omega\chi\varphi(\chi\rho_b,\chi R_c)}{\pi kT\rho_b^3} \\ &\times\left(1 + \frac{D_{gb}w\Omega\chi\varphi(\chi\rho_b,\chi R_c)}{kT\rho_b u_{gb}}\right)^{-1}\Bigg], \end{aligned} \tag{47}$$

where $\varphi(\chi\rho_b, \chi R_c) = \dfrac{K_1(\chi\rho_b)I_1(\chi R_c) - I_1(\chi\rho_b)K_1(\chi R_c)}{I_0(\chi\rho_b)K_1(\chi R_c) + K_0(\chi\rho_b)I_1(\chi R_c)}$.

In the meaningful limit $R_c \gg w$, $\rho_b \geqslant w$, one has with a very good accuracy $\varphi(\chi\rho_b, \chi R_c) \approx 1$, until $\rho_b < R_c$:

$$v_{gb} = (\Delta G + 2\varepsilon)\pi\rho_b^2 \left[\frac{D_{gb} w \Omega \chi}{\pi k T \rho_b^3}\left(1 + \frac{D_{gb} w \Omega \chi}{k T \rho_b u_{gb}}\right)^{-1}\right]. \quad (48)$$

Superposition of Eqs. (43) and (48) allows exclusion of the parameter ε and final calculation of the grain boundary velocity:

$$v_{gb} = \frac{u_{gb} u_b / n_b}{u_{gb} + u_b / n_b} \Delta G, \quad (49)$$

where the bubble mobility is presented by the expression in brackets of Eq. (48):

$$u_b = \frac{D_{gb} w \Omega \chi}{\pi k T \rho_b^3}\left(1 + \frac{D_{gb} w \Omega \chi}{k T \rho_b u_{gb}}\right)^{-1}. \quad (50)$$

In the limit $\rho_b \to R_c$, corresponding to complete coverage of the grain face by bubbles, $\varphi(\chi\rho_b, \chi R_c) \to 0$ in a steep manner, therefore, the grain boundary velocity in Eq. (47) also turns to zero, $v_{gb} \to 0$, in a qualitative agreement with the prediction of the simplified model, Eq. (28).

A further simplification of Eq. (50) can be attained using evaluation of the grain boundary mobility u_{gb} in Eq. (34) resulting in $\chi \approx w^{-1}$. In this case the bubble mobility can be approximated as

$$u_b = \frac{D_{gb}\Omega}{\pi k T \rho_b^3}\left(1 + \frac{2w}{\rho_b}\right)^{-1} \approx \frac{D_{gb}\Omega}{\pi k T \rho_b^3}. \quad (51)$$

3.3. Discussion

In derivation of Eqs. (49) and (50) it was implicitly assumed that the surface diffusion of uranium atoms along the two segments (upper and lower) of the bubble surface disconnected by the grain boundary, was fast enough to redistribute in the bubble all vacancies absorbed from the upper surface of the grain boundary (flux $J_v^{(1)}$) and desorbed to the lower one (flux $J_v^{(2)}$), in order to sustain its steady-state lenticular shape in the course of grain boundary migration.

This assumption can be explicitly grounded if one compares two expressions for the bubble mobility by the new mechanism, Eq. (51), and by the bubble surface diffusion mechanism. For the spherical intragranular bubbles the latter (which was roughly evaluated in [6]) takes the form (see Appendix B):

$$u_s \approx \frac{3 D_s a \Omega}{2\pi k T R_b^4}, \quad (52)$$

where D_s is the surface diffusion coefficient of uranium atoms over the bubble surface, R_b is the radius of the spherical bubble, $a \approx w$ is the thickness of the surface layer.

For the lenticular grain face bubble the mobility by the surface diffusion mechanism (i.e. under assumption that the atomic transport between the two segments of the bubble surface across the grain boundary is not a rate-limiting process) is presented by a similar to Eq. (52) relationship, derived in Appendix B:

$$u_s \approx \frac{3 D_s w \Omega}{2\pi k T \rho_b^4} \frac{\sin^4\theta_0}{1 - \cos^3\theta_0} \approx \frac{3 D_s w \Omega}{4\pi k T \rho_b^4}, \quad (53)$$

where $\theta_0 \approx \theta_1 \approx \theta_2 \approx 50°$.

Therefore, comparing Eqs. (51) and (53) one can see that $\frac{u_b}{u_s} \approx \frac{D_{gb}}{D_s}\frac{\rho_b}{w}$. From analysis of experimental data for D_{gb} [17] and for D_s [18,19] one can conclude that D_s exceeds D_{gb} by 1–2 orders of magnitude in a wide range of temperatures above 1000 K, increasing with temperature. At higher temperatures $T \approx 2000$ K, when the grain growth becomes noticeable, the ratio D_s/D_{gb} attains three orders of magnitude. Therefore, for the practical interval of bubble sizes $w \leqslant \rho_b \leqslant 10^3 w$, i.e. from $\approx$1 nm up to $\approx$1 μm, the ratio u_b/u_s is still small.

This confirms that the new mechanism of bubble migration is significantly slower than the standard bubble surface diffusion mechanism and thus is the rate determining step in the migration process (under assumption that the two other mechanisms of bubble migration by gas transport in the bubble and volume diffusion in the surrounding solid matrix are much slower).

In this case diffusion fluxes of uranium atoms $\vec{I}_s(\theta)$ over the two surfaces of the lenticular bubble should provide relocation of each surface segment with the velocity $v_b = v_{gb}$, in accordance with the relationship valid for spherical surfaces [20] and thus also for any segment of a spherical surface:

$$\vec{v}_b \cdot \vec{n} = \Omega \vec{\nabla}_s \cdot \vec{I}_s, \quad (54)$$

where $\vec{n}(\theta)$ is the unit vector in the normal to the surface direction.

Solution of Eq. (54) for the absolute value of the vector $\vec{I}_s(\theta)$ directed along the bubble surface is

$$I_s^{(1,2)}(\theta) = -(v_b R_{1,2}/2\Omega)\sin\theta. \quad (55)$$

Comparing Eq. (55) with Eq. (30), one can see that the flux matches are identically satisfied on the contact line between the bubble and the grain boundary (see Fig. 3):

$$J_v^{(1)} = \pi\rho_b^2 v_{gb}/2\pi\rho_b\Omega = -I_s^{(1)}(\theta_1), \quad (56)$$

and

$$J_v^{(2)} = -\pi\rho_b^2 v_{gb}/2\pi\rho_b\Omega = I_s^{(2)}(\pi - \theta_2), \quad (57)$$

where $R_1 \cdot \sin\theta_1 = R_2 \cdot \sin\theta_2 = \rho_b$, in accordance with Eq. (24).

Therefore, uranium atoms transferred from one grain into another by the atomic jumps under the chemical

potential gradient across the grain boundary, are redistributed among the grain boundary and the attached bubbles by the surface diffusion along the grain boundary (D_{gb}). Further transport of atoms along the bubble surface (disconnected into two segments by the grain boundary) is sustained by a more rapid diffusion process on the bubble surfaces (D_s), which preserves the bubble steady-state shape in the course of coherent relocation of the grain boundary and the attached bubble.

4. Model validation

The new grain growth model was implemented in the MFPR code [7–9] and used to simulate the data of steady irradiation tests of Turnbull [10]. In these experiments the grain growth kinetics of uranium dioxide under steady irradiation conditions was studied. Small cylindrical specimens 10 mm long and 3 mm diameter were prepared from 2% enriched uranium dioxide of near theoretical density. The fuel samples were irradiated at $T = 2023$ K for period of 2, 4 and 6 months in UKAEA reactor DIDO in a flux of $\approx 2.4 \times 10^{17}$ thermal neutrons/m^2 s. There were three types of samples with the initial grain diameter $d_{gr} = 7$ μm (specimens A and B) and 40 μm (specimen C), the latter being produced by preliminary annealing of specimens A during 72 h at $T = 1973$ K in hydrogen. Specimens B and C were pre-irradiated to 0.02% burn-up at 353 K. So, the following identification of the specimens is used:

- specimen A, 7 μm starting grain size;
- specimen B, 7 μm starting grain size, pre-irradiated to 0.02% burn-up at 353 K;
- specimen C, 40 μm starting grain size, pre-irradiated to 0.02% burn-up at 353 K.

Examination of large-grained specimen C showed the unchanged average grain size, whereas specimens A and B exhibited identical grain growth characteristics with the grain size increasing from 7 μm to 18 μm after 6 months irradiation.

In order to simulate the tests with the MFPR code, at first parameters of Eq. (48) for the normal grain growth kinetics in non-irradiated fuel represented in the standard form:

$$v_{gb}^{(0)} = v_0 \left(\frac{d_0}{d_{gr}}\right)^n \exp(-E_{gb}/T), \tag{58}$$

were fitted to reproduce the out-of-pile annealing behaviour of specimen C. Since the density of the samples was close to theoretical one, the parabolic kinetics for normal grain growth with parameters $n = 1$, $v_0 = 1.4$ m/s, $d_0 = 7$ μm and activation energy $E_{gb} = 44\,200$ K recommended by Speight–Greenwood [1] was assumed in calculations.

The MFPR code allows mechanistic calculation of fission gas atoms and intragranular bubbles migration to and sweeping by moving grain boundaries, which feed formation and growth of intergranular bubbles. Various types of intergranular bubbles (grain face, edge and corner) with different drag forces are considered as described in Section 2. However, the new mechanism of the intergranular bubble migration is currently applied only to the face bubbles, whereas migration of the peripheral edge and corner bubbles is considered in the standard approach (i.e. by the surface diffusion mechanism). Apparently this turns out in some underestimation of the peripheral bubbles input in the total drag force exerted on the grain boundary. Extension of the new model to consideration of this effect was recently carried out and, after implementation in the code, improved results will be published elsewhere. The mean surface concentration of face bubbles was estimated as $\approx 4 \times 10^{10}$ m^{-2} from the post-test fracture surface image presented in [10] and used in the calculations as a fixed value, whereas variation of their mean size owing to absorption of gas atoms from grains was calculated by the code.

The MFPR code with the fixed parameters of the new model was applied to simulation of grain growth of the specimens A, B and C under irradiation. In the standard approach using bubble mobility u_s determined by the bubble surface diffusion mechanism, Eq. (52), calculations strongly overpredict the measured grain growth for all three specimens, Fig. 4.

In the new approach the bubble mobility $\tilde{u}$ was calculated as the minimum between the two values u_b and u_s determined by the grain boundary diffusion and bubble surface diffusion mechanisms, Eqs. (51) and (53), respectively, i.e. $\tilde{u} = \min(u_b, u_s)$. Comparing parameters of

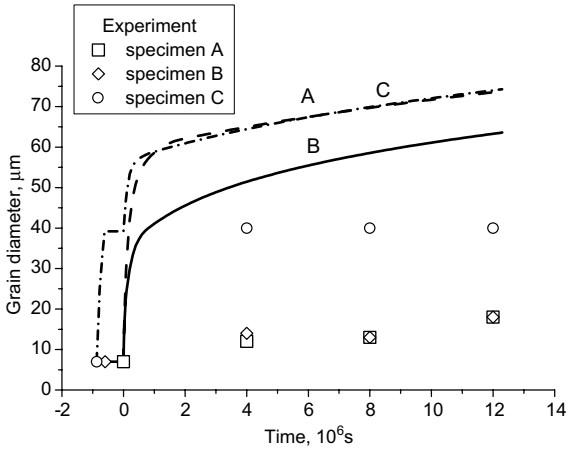

Fig. 4. Simulation of the Turnbull's tests [10] with the MFPR code using the standard mechanism (bubble surface diffusion) for the mobility of grain face bubbles.

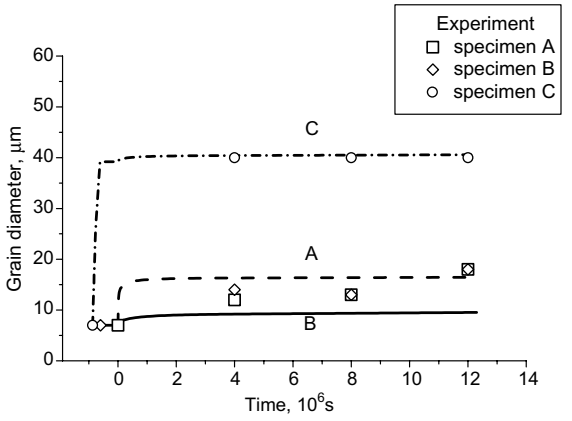

Fig. 5. Simulation of the Turnbull's tests [10] with the MFPR code using the basic version of the new model for the mobility of grain face bubbles with $D_{\rm gb}^{(l)} = 4 \times 10^{-6} \exp(-44\,200/T)$ m^2/s.

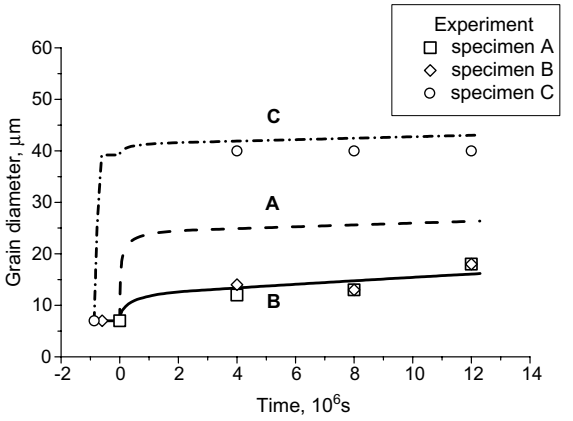

Fig. 6. Simulation of the Turnbull's tests [10] with the MFPR code using modification of the new model for the mobility of grain face bubbles with $D_{\rm gb}^{(l)} = 4 \times 10^{-6} \exp(-35\,250/T)$ m^2/s.

Eqs. (33) and (34) with the above presented parameters of Eq. (58), one can estimate the value of the grain boundary diffusion coefficient $D_{\rm gb}$ from Eq. (34) and then use this value for determination of the bubble mobility $u_{\rm b}$ in Eq. (51).

In this approach the new model predicts a rather good agreement for the samples B and C and slightly overpredicts the growth of the sample A, Fig. 5. However, as indicated by Turnbull [10], his result concerning negligible effect of pre-irradiation on grain growth (i.e. identical grain growth of the samples A and B) was in contradiction with the test of MacEwan and Hayashi [11], who reported that a similar to specimen B 'cold' pre-irradiation of samples was sufficient to arrest grain growth at high temperatures ≈2073 K. In this respect the new model is in qualitative agreement with the latter observations.

It should be noted that the above estimated value of the grain boundary diffusion coefficient $D_{\rm gb} \approx 4 \times 10^{-6} \exp(-44\,200/{\rm T})$ m^2/s (obtained by comparison of Eqs. (33) and (34) with Eq. (58)) at the test temperature ≈2023 K turns to be one order of magnitude smaller than the value directly measured by Alcock et al. [17]. This contradiction can be explained by an assumption that the grain boundary diffusivity (as well as other material properties) may change with burnup, or by an additional assumption that the diffusivity along the grain boundary measured in [17], $D_{\rm gb}^{(l)} \approx 4 \times 10^{-6} \exp(-35\,250/{\rm T})$ m^2/s, differs from the diffusivity across the grain boundary evaluated in Eq. (34) following Burke and Turnbull [12], $D_{\rm gb}^{(p)} \approx 4 \times 10^{-6} \exp(-44\,200/T)$ m^2/s.

Under the latter assumption Eq. (50) takes the form $u_{\rm b} = \frac{D_{\rm gb}^{(l)} w \Omega \chi}{\pi k T \rho_{\rm b}^3}$, where $\chi = \sqrt{2 u_{\rm gb} k T / D_{\rm gb}^{(l)} w \Omega}$ and $u_{\rm gb} \approx \frac{D_{\rm gb}^{(p)} \Omega}{2 w k T}$, i.e. $\chi = \frac{1}{w}\sqrt{D_{\rm gb}^{(p)}/D_{\rm gb}^{(l)}}$. Therefore, instead of Eq. (51) one gets a modified expression for the bubble mobility:

$$u_{\rm b} \approx \frac{\Omega}{\pi k T \rho_{\rm b}^3} \sqrt{D_{\rm gb}^{(p)} D_{\rm gb}^{(l)}}. \tag{59}$$

In this case the model predictions, Fig. 6, are not as good as in the previous case, but are still reasonable, taking into account accuracy limits of the tests [10]. Nevertheless, even in this case a substantial improvement of the code predictions in comparison with the standard approach, Fig. 4, is apparent.

Further improvement of calculation results can be apparently attained by additional consideration of solid precipitates formed on the grain boundaries under irradiation, which exert an additional drag force on the grain boundary unaccounted in the current model.

Being applied to the tests of MacEwan and Hayashi [11], the model allows a reasonable simulation of the observed grain growth during post-irradiation annealing of uranium dioxide. In these tests the effect of prior exposure to irradiation at temperature below 673 K on subsequent grain growth of UO_2 samples with densities from 94% to 96% of theoretical density at 2073 K during 24 h was studied, as shown in Fig. 7. Growth was reduced in all irradiated specimens, with nearly complete inhibition occurring by 4×10^{19} fissions/cm^3 (corresponding to 80 days of irradiation).

In MFPR calculations the normal grain growth velocity was adjusted to the test data for non-irradiated samples, whereas all further calculations for pre-irradiated samples were performed with the fixed set of the model parameters, similar to that used in calculations in Fig. 6. Results of these calculations are presented in Fig. 7 (solid line) and demonstrate a reasonable agreement with experimental data.

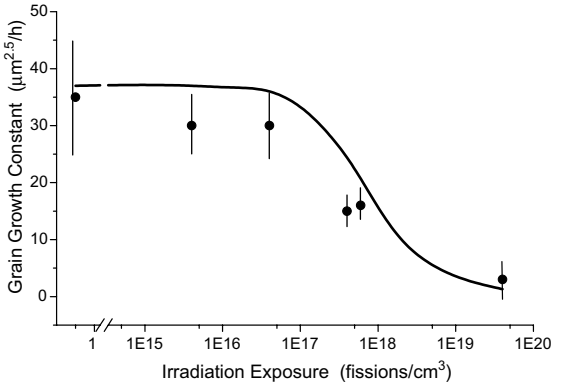

Fig. 7. Simulation of the MacEwan and Hayashi's tests [11], with the MFPR code using the same set of the model parameters as in Fig. 6. Pre-irradiation temperature: 673 K; annealing temperature: 2073 K; annealing time: 24 h.

5. Conclusions

A new model for the grain growth in irradiated and non-irradiated UO_2 pellets is developed.

As the first step of the new model development, Nichols' approach [4] to consideration of the drag force exerted by attached bubbles and pores on migrating grain boundaries is combined with supplementary consideration of grains coalescence within Hillert's mean field approach [5]. It is shown that the boundary migration rate becomes controlled by the movement of the second-phase particles with significantly smaller sizes than predicted in the simplified approach [4]. An additional consideration recommended by Rest [3] of various types of grain boundary pores and bubbles (i.e. grain face, edge and corner) which exert different drag forces owing to their different shapes and sizes, is performed in the model.

On the other hand, Nichols' analysis [4] is based on consideration of retarding effect using the standard (surface diffusion) mechanisms of bubble mobility derived for intragranular bubbles. This mechanism was re-considered in the present paper taking into account a more complicated, lenticular, shape of the grain face bubbles. However, besides this, migration mechanism of the grain face bubbles might be essentially different from the intragranular bubbles, owing to their specific location on and interaction with a grain boundary. The new mechanism of the lenticular grain face bubble migration is associated with vacancy fluxes over the grain boundary surfaces to the bubble, which afford coherent relocation of the grain boundary-bubble complex. The calculated mobility of the grain face bubble is characterised by a slower dependence on its projected radius, $\propto \rho_b^{-3}$, in comparison with the surface diffusion mechanism, $\propto \rho_b^{-4}$, which sustains its steady-state lenticular shape in the course of bubble migration. For this reason, the new mechanism becomes the rate controlling step for bubbles migration in a wide range of their radii from $\sim$1 nm to $\sim$1 μm, and correspondingly, determines the drag force exerted by bubbles on the grain boundary.

The model is implemented in the MFPR code which is designed for modelling fission product release from irradiated UO_2 fuel, and validated against tests on grain growth kinetics during steady irradiation exposure [10] and during post-irradiation annealing [11] of fuel samples. Results of calculations are in a reasonable agreement with the test data and allow explanation of the strong retarding effect of irradiation on the grain growth observed in these tests.

Acknowledgements

This work was supported by IRSN, Cadarache (France) under the Contract No. MFPR 2005 on the mechanistic code MFPR development; the personal support and collaboration of Drs R. Dubourg and P. Giordano (IRSN) are highly appreciated. The author also thanks Dr V. Tarasov and Mr D. Antropov (IBRAE) for their assistance in implementation of the new model in the MFPR code.

This work was also supported by the Russian Foundation for Basic Research which is greatly acknowledged by the author.

Appendix A

In this appendix will be searched the solution of Eq. (44):

$$\frac{D_{gb} w \Omega}{kT} \nabla_s^2 \mu_1 + \frac{u_{gb}(\mu_2 - \mu_1)}{\Omega} - v_{gb} = 0, \tag{A.1}$$

$$\frac{D_{gb} w \Omega}{kT} \nabla_s^2 \mu_2 - \frac{u_{gb}(\mu_2 - \mu_1)}{\Omega} + v_{gb} = 0, \tag{A.2}$$

with the boundary conditions, Eq. (45):

$$\left(\frac{d\mu_{1,2}}{dr}\right)_{r=R_c} = 0 \quad \text{and} \quad \mu_{1,2}(\rho_b) = \left(\frac{2\gamma_s}{R_{1,2}} - p_b\right)\Omega. \tag{A.3}$$

The sum of Eqs. (A.1) and (A.2) results in the Laplace type equation for a variable $\mu_1 + \mu_2$:

$$\Delta_s(\mu_1 + \mu_2) = 0,$$

which under condition of a cylindrical symmetry around a bubble in its occupation region $r \leqslant R_c$ has a general solution:

$$\mu_1 + \mu_2 = A + B \ln r, \tag{A.4}$$

whereas the difference of Eqs. (A.1) and (A.2) results in the Helmholtz type equation for a variable $x(r) = \mu_2 - \mu_1 - v_{gb}\Omega/u_{gb}$:

$$\Delta_s x - \chi^2 x = 0, \tag{A.5}$$

with $\chi = \sqrt{2u_{gb}kT/D_{gb}w\Omega^2}$, which has a general solution with the cylindrical symmetry:

$$x = CI_0(\chi r) + DK_0(\chi r),$$

or

$$\mu_2 - \mu_1 = v_{gb}\Omega/u_{gb} + CI_0(\chi r) + DK_0(\chi r). \tag{A.6}$$

Superposition of Eqs. (A.4) and (A.6) yields the searched solution:

$$2\mu_1 = A + B\ln r - v_{gb}\Omega/u_{gb} - CI_0(\chi r) - DK_0(\chi r), \tag{A.7}$$

$$2\mu_2 = A + B\ln r + v_{gb}\Omega/u_{gb} + CI_0(\chi r) + DK_0(\chi r), \tag{A.8}$$

where the constants are found out by substitution of Eqs. (A.7) and (A.8) in the boundary conditions, Eq. (A.3):

$$B = 0, \quad A = 2\left(\frac{\gamma_s}{R_1} + \frac{\gamma_s}{R_2} - p_b\right)\Omega = -\Delta G\Omega,$$

$$D = C\frac{I_1(\chi R_c)}{K_1(\chi R_c)},$$

$$C = \frac{\dfrac{2\gamma_s}{R_2} - \dfrac{2\gamma_s}{R_1} - v_{gb}/u_{gb}}{I_0(\chi\rho_b) + K_0(\chi\rho_b)I_1(\chi R_c)/K_1(\chi R_c)} = \frac{\Delta G + 2\varepsilon - v_{gb}/u_{gb}}{I_0(\chi\rho_b) + K_0(\chi\rho_b)I_1(\chi R_c)/K_1(\chi R_c).} \tag{A.9}$$

Appendix B

In this appendix the mobility of a lenticular grain face bubble by the surface diffusion mechanism is calculated, which is valid under assumption that the atomic transport between the two segments of the bubble surface across the grain boundary is not a rate-limiting process.

Let us consider two bubbles: a lenticular bubble consisting of two segments of spherical surfaces with close radii $R_1 \approx R_2$ and contact angles $\theta_1 \approx \theta_2 \approx \theta_0 \approx \arccos(\gamma_{gb}/2\gamma_s) \approx 50°$, and a spherical bubble with a radius $R \approx R_1 \approx R_2$, moving with the same velocity v_b. A similar flux distribution over the lenticular bubble surface and over two surface segments of the spherical bubble in the range $0 < \theta < \theta_1$ and $0 < \pi - \theta < \theta_2$, which provides relocation of these two bubbles with the same velocity v_b (see Eq. (54)), can be induced by a similar normal stress distribution $\sigma_{rr}(\theta)$ over these surfaces in the surrounding solid matrix:

$$I_s(\theta) = -\frac{D_s a}{\Omega kT}\nabla_s\mu_s(\theta) = -\frac{D_s a}{kT}\nabla_s\sigma_{rr}(\theta), \tag{B.1}$$

where $\mu_s(\theta) = \mu_0 + \sigma_{rr}(\theta)\Omega$, and $\nabla_s(\cos\theta) = R^{-1}\sin\theta$.

Comparing Eq. (B.1) with Eq. (55), one can see that:

$$\sigma_{rr}(\theta) = \frac{v_b R^2 kT}{2D_s a\Omega}\cos\theta. \tag{B.2}$$

This implies that the net external force acting on the spherical bubble is equal to:

$$F_{sph} = \int_0^\pi \sigma_{rr}\cos\theta\,dS = \frac{2\pi R^4 kT}{3D_s a\Omega}v_b, \tag{B.3}$$

whereas the net force acting on the lenticular bubble surface is equal to:

$$F_{lent} = \int_0^{\theta_1}\sigma_{rr}\cos\theta\,dS + \int_{\pi-\theta_2}^{\pi}\sigma_{rr}\cos\theta\,dS \approx \frac{2\pi R^4 kT(1-\cos^3\theta_0)}{3D_s a\Omega}v_b \approx \frac{2\pi\rho_b^4 kT}{3D_s a\Omega}\frac{(1-\cos^3\theta_0)}{\sin^4\theta_0}v_b. \tag{B.4}$$

Therefore, for the bubble mobility $u_b = v_b/F$ one obtains the above presented Eqs. (52) and (53).

The data for the surface diffusion coefficient compiled by Maiya [18] and Matzke [19] give the following relationship for the surface diffusion coefficient of uranium atoms:

$$D_s = 50\exp(-450{,}000/RT)(m^2/s), \tag{B.5}$$

with 1200 °C < T < 1800 °C and R in J mol^{-1} K^{-1}.

References

[1] M.V. Speight, G.W. Greenwood, Philos. Mag. 9 (1964) 683.
[2] T.J. Heames, D.A. Williams, N.E. Bixler, A.J. Grimley, C.J. Wheatley, N.A. Johns, P. Domogala, L.W Dickson, C.A. Alexander, I. Osborn-Lee, S. Zawadzki, J. Rest, A. Mason, R.Y. Lee, VICTORIA: A Mechanistic Model of Radionuclide Behaviour in the Reactor Coolant System under Severe Accident Conditions, NUREG/CR-5545, 1992.
[3] J. Rest, J. Nucl. Mater. 131 (1985) 291.
[4] F.A. Nichols, J. Am. Ceram. Soc. 51 (1968) 468.
[5] M. Hillert, Acta Metall. 36 (1965) 469.
[6] P.G. Shewmon, Trans. AIME 230 (1964) 1134.
[7] M.S. Veshchunov, A.V. Berdyshev, V.D. Ozrin, V.E. Shestak, V.I. Tarasov, in: Proc. Int. Conf. 'TopFuel 2003: Nuclear Fuel for Today and Tomorrow. Experience and Outlook', Würzburg, Germany, 16–19 March 2003.
[8] R. Dubourg, G. Nicaise, in: Proc. Int. Conf. 'TopFuel 2003: Nuclear Fuel for Today and Tomorrow. Experience and Outlook', Würzburg, Germany, 16–19 March 2003.
[9] M.S. Veshchunov, V.D. Ozrin, V.E. Shestak, V.I. Tarasov, R. Dubourg, G. Nicaise, in: Proc. 2004 Int. Meeting on LWR Fuel Performance Orlando, Florida, 19–22 September 2004, Paper 1085.
[10] J.A. Turnbull, J. Nucl. Mater. 50 (1974) 62.

[11] J.R. Mac Ewan, J. Hayashi, Proc. Br. Ceram. Soc. 7 (1965) 245.
[12] J.E. Burke, D. Turnbull, Prog. Metal Phys. 3 (1952) 220.
[13] G.W Greenwood, Acta Met. 4 (1956) 243.
[14] I.M. Lifshitz, V.V. Slyozov, Zh. Eksp. Teor. Fiz. 35 (1958) 479.
[15] D.G. Cole, P. Feltham, E. Gilliam, Proc. Phys. Soc. B 67 (1954) 131.
[16] M.V. Speight, W. Beere, Metal Sci. 9 (1975) 190.
[17] G.B. Alcock, R.J. Hawkins, A.W.D. Hills, P. McNamara, Paper SM-66/36, IAEA, Symp. Thermodynamics, Vienna, 1965, p. 57.
[18] P.S. Maiya, J. Nucl. Mater. 40 (1971) 57.
[19] Hj Matzke, in: L.C. Dufour, J. Novotny (Eds.), Surfaces and Interfaces of Ceramic Materials, Kluwer Academic, Dordrecht, 1989, p. 241.
[20] Ya.E. Geguzin, M.A. Krivoglaz, Migration of Macroscopic Precipitates in Solid Materials, Moscow, 1971 (in Russian).